

Methyl formate as a hydrogen energy carrier

Received: 13 August 2022

Accepted: 11 April 2023

Published online: 22 June 2023

Check for updates

Rui Sang^{1,5}, Zhihong Wei^{2,5}, Yuya Hu^{1,5}, Elisabetta Alberico^{1,3}, Duo Wei¹, Xinxin Tian², Pavel Ryabchuk¹, Anke Spannenberg¹, Rauf Razzaq¹, Ralf Jackstell¹, Jonas Massa⁴, Peter Sponholz⁴, Haijun Jiao¹, Henrik Junge¹ & Matthias Beller¹

The use of renewable energy is central for the realization of a circular economy, which is essential for further global economic development. In this background, hydrogen storage materials play an important role. Here we propose a previously overlooked, industrially available bulk chemical (methyl formate, MF) as an efficient and practical hydrogen storage material. Utilizing appropriate catalysts, hydrogen production from MF is significantly faster than with other established chemical hydrogen carriers, such as formic acid and methanol, under very mild conditions. The optimized MF dehydrogenation system presented here is highly active (maximum turnover frequency (TOF_{max}) $> 44,000 \text{ h}^{-1}$ and turnover number $> 100,000$) and selective (CO undetectable). Moreover, the solvent-free MF dehydrogenation demonstrates its application potential. Here we show the dehydrogenation reaction of MF. We expect that these insights will serve as an inspiration for the development of alternative energy materials and new catalytic transformations.

The improvement of our current energy technologies in terms of sustainability for future human development represents one of the global challenges of the twenty-first century^{1,2}. With the aim of replacing fossil fuels and decreasing the anthropogenic emissions of CO_2 , worldwide efforts to utilize renewable energy are currently under way. Both the Paris and more recent Glasgow Agreements aim to avoid global warming and mitigate climatic changes via net-zero CO_2 emissions. The necessary paradigm shift of our present energy system can be achieved through the transformation of renewable wind, solar or hydro power to better storable chemical fuels^{3,4}. In this respect, hydrogen is considered to be a promising chemical energy carrier⁵ that could be produced from renewable resources, for example, via electrochemical water splitting^{6,7}. Indeed, the global hydrogen market is expected to reach around US\$700 billion by 2050^{8,9}. However, its chemical and physical properties, for example, its low volumetric energy content at ambient conditions ($0.0023 \text{ kWh l}^{-1}$), its flammability and its explosive nature in oxygen-containing mixtures make its handling, storage and transportation cumbersome, energy-intensive and expensive, especially for long-term/long-distance applications^{10–13}. Both the development of a

chemical hydrogen economy and the exploration/discovery of alternative hydrogen energy carriers thus continue to attract a substantial amount of attention^{14–26}.

An ideal chemical hydrogen source should fulfil the following requirements: it should have high gravimetric and volumetric energy density, low toxicity, fit the present infrastructure, be practical in terms of handling and transportation, and the hydrogen should be cost- and energy-efficient to store as well as release. However, none of the current chemical hydrogen carriers fulfil all these prerequisites. For example (Fig. 1a), methanol²² (MeOH) and ammonia²⁷ are available on a bulk scale and possess a high hydrogen content, but they are classified as toxic and flammable according to the globally harmonized system of classification and labelling of chemicals (GHS^[ECL]) of the United Nations (Fig. 1d)²⁸. Liquid organic hydrogen carriers (LOHCs)²⁹ based on arenes have medium hydrogen densities (5.8–7.3 wt%) and can be easily handled, but are less available and have toxicity problems (Fig. 1d). Formic acid (FA)¹⁷ is directly available from CO_2 , has favourable thermodynamic data (Fig. 1c) and can be easily dehydrogenated even under ambient conditions, but it has a

¹Leibniz-Institut für Katalyse, Rostock, Germany. ²Institute of Molecular Science, Key Laboratory of Materials for Energy Conversion and Storage of Shanxi Province, Key Laboratory of Chemical Biology and Molecular Engineering of Ministry of Education, Shanxi University, Taiyuan, P. R. China. ³Istituto di Chimica Biomolecolare, Consiglio Nazionale delle Ricerche, Sassari, Italy. ⁴APEX Energy Teterow GmbH, Rostock-Laage, Germany. ⁵These authors contributed equally: Rui Sang, Zhihong Wei, Yuya Hu. ✉e-mail: haijun.jiao@catalsos.de; henrik.junge@catalsos.de; matthias.beller@catalsos.de

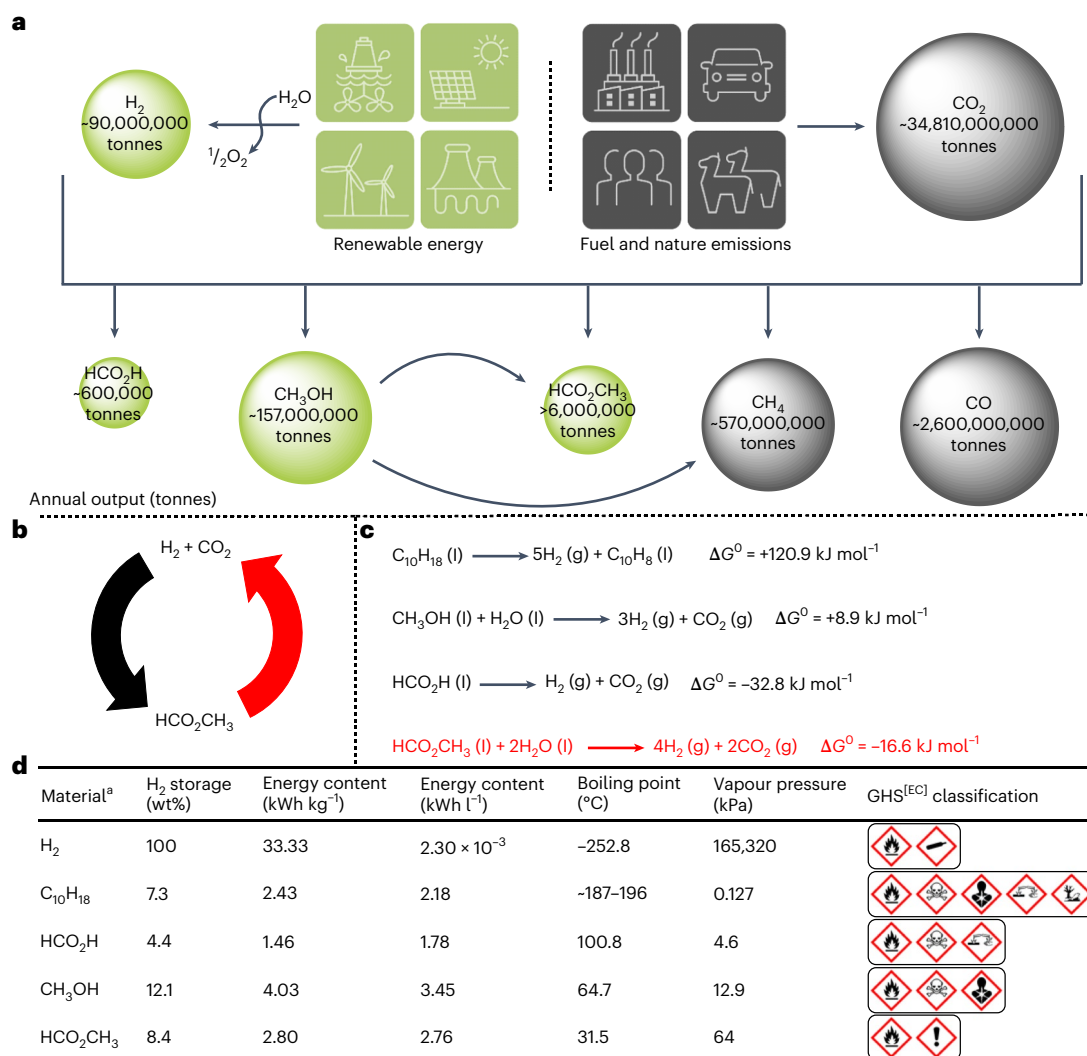


Fig. 1 | Selected hydrogen energy systems. a, Energy carriers based on CO₂ (the values in tonnes represent annual output from industry and nature emission). **b**, Using MF as a chemical hydrogen energy carrier (red indicates this work).

c, Selected catalytic dehydrogenation reactions (red indicates this work). **d**, Properties of different hydrogen energy carriers. ^aThe data are based on the actual dehydrogenation chemical equations in **c**.

low hydrogen content (<5 wt%) and is corrosive (Fig. 1d). This means that there is still strong interest in new practical hydrogen vectors that avoid the abovementioned problems. Methyl formate (MF) drew our particular attention. As shown in Fig. 1d, MF has a hydrogen storage capacity (8.4 wt%) between those of MeOH (12.1 wt%) and FA (4.4 wt%) and comparable to other LOHCs. More specifically, the volumetric energy density of MF is equivalent to pressurized hydrogen at 1,200 bar. Notably, its dehydrogenation is thermodynamically favoured compared to other hydrogen carriers, except FA (Fig. 1c). Furthermore, MF is classified as non-toxic, non-irritating and non-corrosive (Fig. 1d), and it can easily be transported, refuelled and handled. At present, MF is produced industrially from MeOH carbonylation, and the global capacity of MF was >6 million metric tonnes per annum in 2016^{30,31}. In recent years, many research groups, including industry, have demonstrated the possibility of accessing MF through the hydrogenation of CO₂ in the presence of MeOH, which can also be generated utilizing CO₂ (refs. 32–41). Overall, this will allow for sustainable MF synthesis.

Taking all these facts into account, MF seems to be a promising hydrogen carrier, although, surprisingly, and to the best of our knowledge, it has not been proposed or described for this purpose yet. In addition, no precedent for MF dehydrogenation has been reported before (Fig. 1b).

Results

Catalytic MF dehydrogenation

Hydrogen generation from MF is possible in the presence of a number of ruthenium pincer catalysts, as found in previous works on FA and MeOH dehydrogenation^{17,21,22,42–45}. Among the tested catalysts (Table 1; for gas evolution curves see Supplementary Table 2), complexes **C1–C5**, including commercial ones, showed high productivity, with a hydrogen turnover number (TON(H₂)) of up to 21,500, and high activity, with a hydrogen turnover frequency (TOF(H₂))_{max} of up to 8,300 h⁻¹. It is noteworthy that the CO content in the produced gas was <10 ppm when using **C1–C5**, which indicates a highly selective conversion of MF to hydrogen and CO₂. **C2** was chosen as the catalyst for further investigation due to its good performance and commercial availability. The reaction parameters, such as the amount of water, solvent, type and amount of base, and reaction temperature were studied in more detail (Supplementary Tables 3–7). First, the amount of water was varied (Supplementary Table 3), finding an optimal water range of 2–4 equiv. to MF. Notably, an insufficient amount of water led to more CO generation. Second, with the exception of acetonitrile, the use of co-solvents, such as tetrahydrofuran (THF), dioxane, *N,N*-dimethyloctylamine (DMOA) and dimethylformamide (DMF), provided similar hydrogen volumes (Supplementary Table 4). Regarding the base, KOH, NaOH, CsOH, K₂HPO₄ and K₃PO₄ are all appropriate for MF dehydrogenation;

Table 1 | Ru-catalysed MF dehydrogenation

$$\text{HCO}_2\text{CH}_3 + \text{H}_2\text{O} \xrightarrow[\text{Triglyme (10 ml), 90 }^\circ\text{C, 20 h}]{\text{Cat. (0.005 mol\%), KOH (10 mmol)}} \text{H}_2 + \text{CO}_2$$

84 mmol 168 mmol

C1

C2

C3

C4

C5

C6

C7

C8

Entry	Cat.	Δp (bar)	V (ml)	H ₂ :CO ₂ (%)	CO (ppm)	TON(H ₂)	TOF(H ₂) _{max} (h ⁻¹)
1	C1	37.4	3,540	58:42	<10	20,968	5,286
2	C2	38.1	3,645	58:42	<10	21,590	5,677
3	C3	33.9	3,163	58:42	<10	19,058	3,643
4	C4	36.9	3,488	57:43	<10	20,304	4,312
5	C5	38.0	3,564	57:43	Undetectable	20,746	8,376
6	C6	17.3	1,542	57:43	227	8,976	4,171
7	C7	3.9	230	56:44	2,672	1,315	408
8	C8	20.0	1,768	57:43	270	10,292	1,999
9	–	2.1	36	65:33	18,684	–	–

General conditions: under an Ar atmosphere, in a 100-ml autoclave, 4 μmol Ru-catalyst (0.005 mol%, 48 ppm), 10 mmol KOH (0.561 g), 10.0 ml of triglyme, 84 mmol MF (5.2 ml), 168 mmol H₂O (3.0 ml), 90 °C and 20 h. The autoclave was cooled to room temperature and the pressure was carefully released to a manual burette. The content of the gas phase was analysed by GC. Additionally, captured CO₂ was collected in a burette by adding an aqueous solution of HCl to the reaction mixture. All experiments were performed at least twice, and the average gas pressures and values are shown with standard deviations <5%.

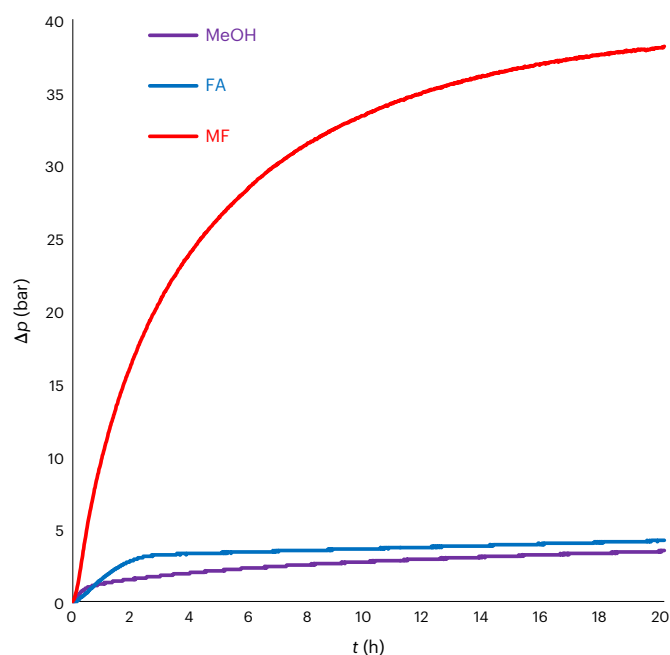
among these, KOH and K₃PO₄ performed best (Supplementary Table 5). Varying the amount of KOH in the range 0–60 mmol revealed an optimal range of 10–40 mmol, which also showed the necessity of the base (Supplementary Table 6). Finally, the reaction temperature was varied from 23 °C to 110 °C (Supplementary Table 7). A temperature between 90 °C and 100 °C led to the best gas evolution, with a CO content below 10 ppm. Notably, MF dehydrogenation is possible even at room temperature. In summary, using MF as a hydrogen carrier allows for hydrogen release under a variety of conditions, which makes it attractive for a number of applications.

Next, we compared the gas evolution rate using MF with established hydrogen energy carriers. MeOH and FA were dehydrogenated under identical mild conditions (Fig. 2). Remarkably, the initial gas evolution rate using MF is five times faster than that with FA and 20 times faster than with MeOH. These unexpected results prompted us to conduct a more in-depth study of the mechanism of MF dehydrogenation.

Mechanistic investigations of MF dehydrogenation

First, the rate of MF dehydrogenation was studied systematically at temperatures between 60 and 90 °C. A linear Arrhenius plot was generated, resulting in an estimated activation energy, E_a , of 65 kJ mol⁻¹ (Fig. 3a). To understand the initial activation step for MF, H₂O was replaced by D₂O, and a secondary kinetic isotope effect (KIE) of $k_{\text{H}}/k_{\text{D}} = 1.40$ was observed (Fig. 3b, entry 2). Notably, a similar KIE ($k_{\text{H}}/k_{\text{D}} = 1.59$) was found when using DCOOCH₃ instead of HCOOCH₃ (Fig. 3b, entry 3). A slightly higher KIE ($k_{\text{H}}/k_{\text{D}} = 1.80$) was obtained with the combination of DCOOCH₃ and D₂O (Fig. 3b, entry 4). These KIE

measurements indicate that the formyl C–H group in MF can be more easily activated compared to the C–H bonds (KIE > 2) in other established hydrogen carriers (MeOH, FA and other LOHCs)^{16,17,21,24,46–49}. To understand this special reactivity, the details of MF dehydrogenation on a molecular level were derived from density functional theory (DFT) calculations. As shown in Fig. 3c and Supplementary Figs. 4–7, starting from the active [KRu–OH] complex with nucleophilic attack of MF, intermediate [KRu–O(H)CHOCH₃] is generated through transition state **TS-MF-OH_k**. After that, hydrogen evolution might occur via two routes: MF direct dehydrogenation (Fig. 3c, red) or MF hydrolysis followed by dehydrogenation (Fig. 3c, blue). In the direct dehydrogenation case, H₂ release proceeds through **TS-CH_k** with a free energy barrier of 80 kJ mol⁻¹ to form the intermediate [KRu–OCOOCH₃], followed by CO₂ release through **TS-CO_{2,k}** to generate the intermediate [KRu–OCH₃]. The alternative MF hydrolysis route resulting in [KRu–OOCH] and CH₃OH formation via transition state **TS-CO_k** has a free energy barrier of 46 kJ mol⁻¹. The following CO₂ and H₂ release via decomposition of [KRu–OOCH] is determined by **TS-H₂/H₂O_k** with a free energy barrier of 124 kJ mol⁻¹, which also leads to the same intermediate [KRu–OCH₃]. Based on these calculations, we propose that H₂ and CO₂ are generated by a direct MF dehydrogenation pathway via the [KRu–OCOOCH₃] intermediate rather than [KRu–OOCH] due to the substantially lower effective energy barrier than that of the MF hydrolysis route (80 versus 124 kJ mol⁻¹). Although the formation of [KRu–OOCH] via the MF hydrolysis route is more favourable than the formation of [KRu–OCOOCH₃] via the MF direct dehydrogenation route, both thermodynamically and kinetically, the release of



General conditions: under Ar atmosphere in a 100-ml autoclave, 4 μmol **C2** catalyst (2.4 mg), 10 mmol KOH (0.561 g), 10.0 ml triglyme, 168 mmol H_2O (3.0 ml), 84 mmol substrate, 90 °C and 20 h.

Fig. 2 | Comparison of MeOH, FA and MF dehydrogenation. Plot of gas evolution (top) and details of the different hydrogen energy carriers and reaction conditions (bottom).

H_2 is the driving force for $[\text{KRu}-\text{OCOOCH}_3]$ formation. Moreover, the decomposition of $[\text{KRu}-\text{OCOOCH}_3]$ is kinetically more favoured than that of $[\text{KRu}-\text{OOCH}]$ (54 versus 124 kJ mol^{-1}). By using the Eyring and Arrhenius equations, the activation energies were calculated based on enthalpy barriers (Supplementary Fig. 7). As shown in Supplementary Table 10, the calculated E_a via the direct dehydrogenation mechanism ($E_a = 61 \text{ kJ mol}^{-1}$) matches the experimentally obtained value of 65 kJ mol^{-1} , which is much lower than that via MF hydrolysis route ($E_a = 121 \text{ kJ mol}^{-1}$). Furthermore, the dehydrogenation of $[\text{KRu}-\text{OCH}_3]$ (free energy barrier of 153 kJ mol^{-1}) is more difficult compared to hydrogen release from $[\text{KRu}-\text{OCOOCH}_3]$. Detailed DFT calculations for MF dehydrogenation in the absence of a base showed the same trend that the direct MF dehydrogenation pathway is more favourable than the MF hydrolysis route (95 versus 129 kJ mol^{-1}), but the effective energy barrier is higher than that under basic conditions by 15 kJ mol^{-1} (Supplementary Figs. 8–11). This is also qualitatively consistent with the experimental results (Supplementary Table 6 entries 1, 3 and 9) that the volume of released H_2 ($V(\text{H}_2)$) for MF as educt in the presence of a base is higher than without a base (3,645 versus 1,820 and 1,980 ml), as well as for HCOOH (359 ml) or MeOH (311 ml) as educts in the presence of a base (Fig. 2 and Supplementary Table 8).

According to the DFT calculations, both $[\text{K}-\text{Ru}-\text{OCOOCH}_3]$ (in the presence of base) and $[\text{H}-\text{Ru}-\text{OCOOCH}_3]$ (base-free conditions) are thermodynamically stable intermediates in the proposed direct MF dehydrogenation pathway. Indeed, it was possible to obtain crystals of the corresponding $[\text{H}-\text{Ru}-\text{OCOOCH}_3]$ complex that were suitable for X-ray analysis (Fig. 3d). When performing the MF dehydrogenation with this defined complex, a pressure curve was observed that is similar

to the one using precursor **C1**, supporting the existence of such active intermediates (Fig. 3e).

To detect other reaction intermediates and further verify the mechanism, a detailed NMR study of MF dehydrogenation was performed. The neutral complex $[\text{H}-\text{Ru}-\text{OH}]$ was prepared by mixing complex **C1** with $t\text{-BuOK}$, followed by celite filtration and adding H_2O (Supplementary Fig. 25). Stoichiometric amounts of ^{13}C -labelled MF ($\text{H}^{13}\text{CO}_2\text{CH}_3$) were then added, and the reaction mixture was analysed by NMR (Supplementary Fig. 34). In agreement with the calculations, the thermodynamically most stable intermediates $[\text{H}-\text{Ru}-\text{OO}^{13}\text{CH}]$ and $[\text{H}-\text{Ru}-\text{O}^{13}\text{COOCH}_3]$ were detected as major products. In addition, $^{13}\text{CO}_2$, $\text{H}^{13}\text{CO}_2\text{CH}_3$, $\text{HCO}_2^{13}\text{CH}_3$, $\text{H}^{13}\text{CO}_2^{13}\text{CH}_3$, HCO_2CH_3 , $^{13}\text{CH}_3\text{OH}$ and CH_3OH were all observed in solution as well as H_2 in the gas phase after the reaction (Supplementary Figs. 30–33). The various ^{13}C -labelled products are explained by the reversible hydrogenation and dehydrogenation reactions, which formally lead to a scrambling of ^{13}C among MF and MeOH (ref. 50). Interestingly, complex $[\text{H}-\text{Ru}-\text{OCH}_3]$, which was assumed to be an important intermediate, was undetectable in the reaction mixture. To understand this observation, a stoichiometric experiment utilizing complex $[\text{H}-\text{Ru}-\text{OCH}_3]$ was performed at room temperature (Supplementary Fig. 35). After adding H_2O , complex $[\text{H}-\text{Ru}-\text{OH}]$ was detected as well as $[\text{H}-\text{Ru}-\text{OCH}_3]$. Both complexes disappeared immediately upon further addition of MF, resulting in the immediate formation of complexes $[\text{H}-\text{Ru}-\text{OOCH}]$ and $[\text{H}-\text{Ru}-\text{OCOOCH}_3]$ (Supplementary Fig. 42). All these NMR studies are in good agreement with the DFT calculations and strongly support the proposed direct MF dehydrogenation pathway.

Finally, a time-resolved analysis of the reaction revealed the consumption of a significant amount of MF (23%), even during the initial heating from room temperature to 90 °C, leading to H_2 , CO_2 , MeOH and FA/formate (Fig. 4a). During this period, the pH changed from 10.9 to 7.4 and then remained constant between 6.8 and 7.6 due to the formation of a buffer system. With ongoing reaction, MF was continuously consumed and the amounts of hydrogen, CO_2 and MeOH were further increased. A maximum amount of FA/formate was detected between 1 and 5 h.

All the mechanistic investigations, including KIE measurements, DFT calculations, crystallization of intermediate $[\text{H}-\text{Ru}-\text{OCOOCH}_3]$, NMR studies and time-resolved analysis, agree with the catalytic cycle shown in Fig. 4b. Initially, under basic conditions, formation of the active species **I** takes place, which, after nucleophilic attack of MF, hydride transfer and H_2 elimination, leads to key intermediate **II**. After release of CO_2 , complex **III** is formed. Subsequently, methoxy and formate group dehydrogenation occur and finally the active catalyst **I** is regenerated. In addition, **I** or **II** can be formed from **III** or **IV** by ligand exchange or via MeOH-assisted MF formation, respectively.

In general, by using 1 mol aqueous MF as a hydrogen carrier, up to four moles of hydrogen and two moles of CO_2 can be generated (Fig. 1c, equation in red). To prove this, and to demonstrate the stability of our catalyst system, we performed several consecutive runs of MF dehydrogenation and gas release by applying 84 mmol MF/168 mmol H_2O (Supplementary Table 19). As the dehydrogenation reaction reaches an equilibrium state in a closed system, the formed gases were released after reaching a pressure plateau. The volumes and gas constitution were measured after each run. The catalyst system was stable for more than 25 consecutive runs, resulting in a gas release of >4.3 l that contained 2.5 l (103 mmol) H_2 , corresponding to a catalyst TON of >25,000. In an additional long-term experiment, >9.4 l of gas, overall, was released, with 60% H_2 yield (241 mmol) based on MF (100 mmol, 6.1 ml; Supplementary Table 20). The detected ratio of H_2 to CO_2 was 1.7:1, which is near the expected ratio ($\text{H}_2/\text{CO}_2 = 2:1$) for MF aqueous reforming as in Fig. 1c. Apart from a continuous supply of hydrogen at low pressure, MF can be used advantageously for the rapid generation of high-pressure

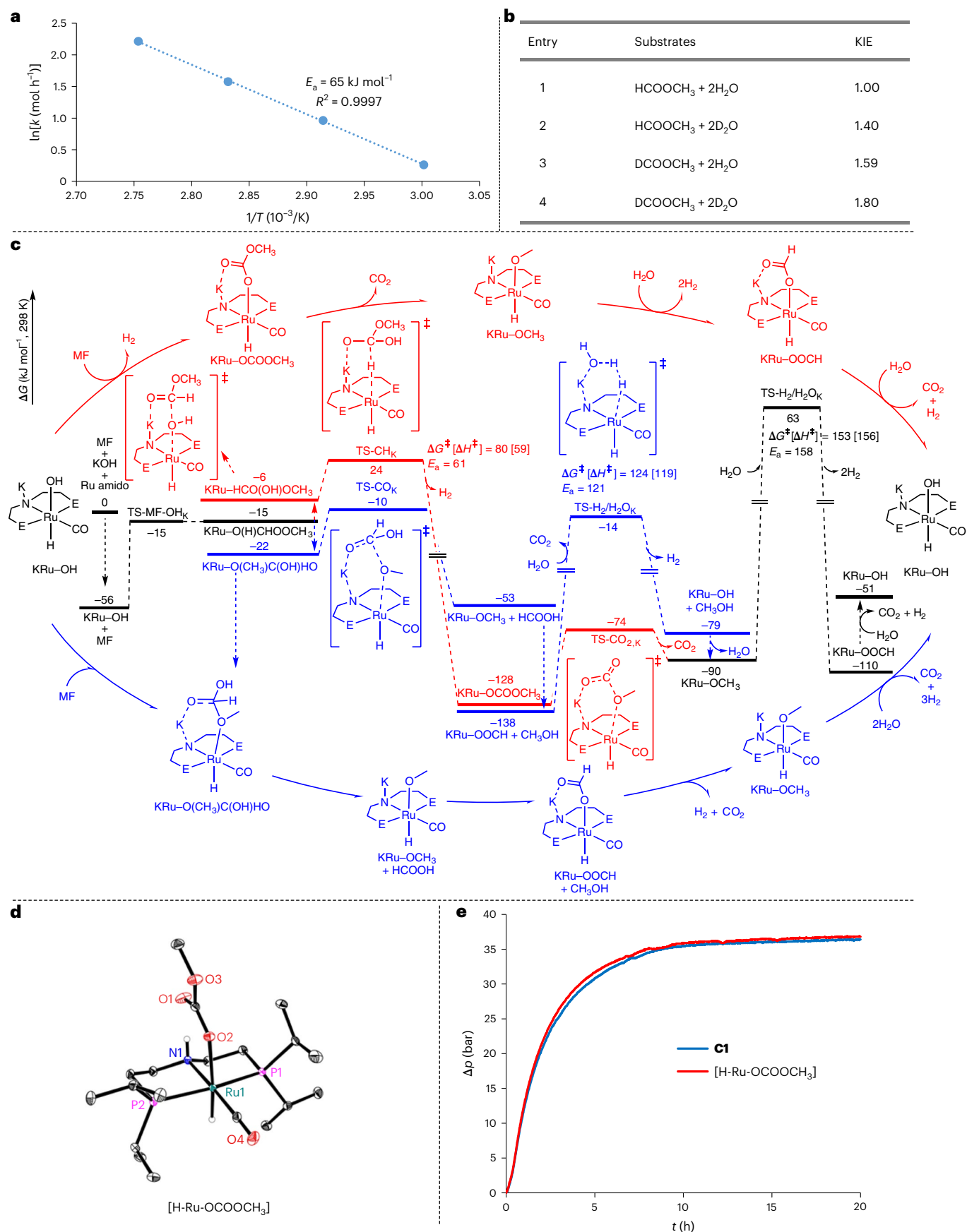


Fig. 3 | Mechanistic investigations of MF dehydrogenation. **a**, Arrhenius plot. **b**, KIE data. For the curve slopes, see Supplementary Table 9. **c**, Molecular details of the DFT calculations. E, PPh₂. Red colour route: MF direct dehydrogenation. Blue colour route: MF hydrolysis followed by dehydrogenation. **d**, Solid-state

structure of the key intermediate [H-Ru-OCOCH₃] without carbon-bound hydrogen atoms. The displacement ellipsoids correspond to 30% probability. **e**, Dehydrogenation comparison using the intermediate crystal [H-Ru-OCOCH₃] and its corresponding catalyst precursor **C1**.

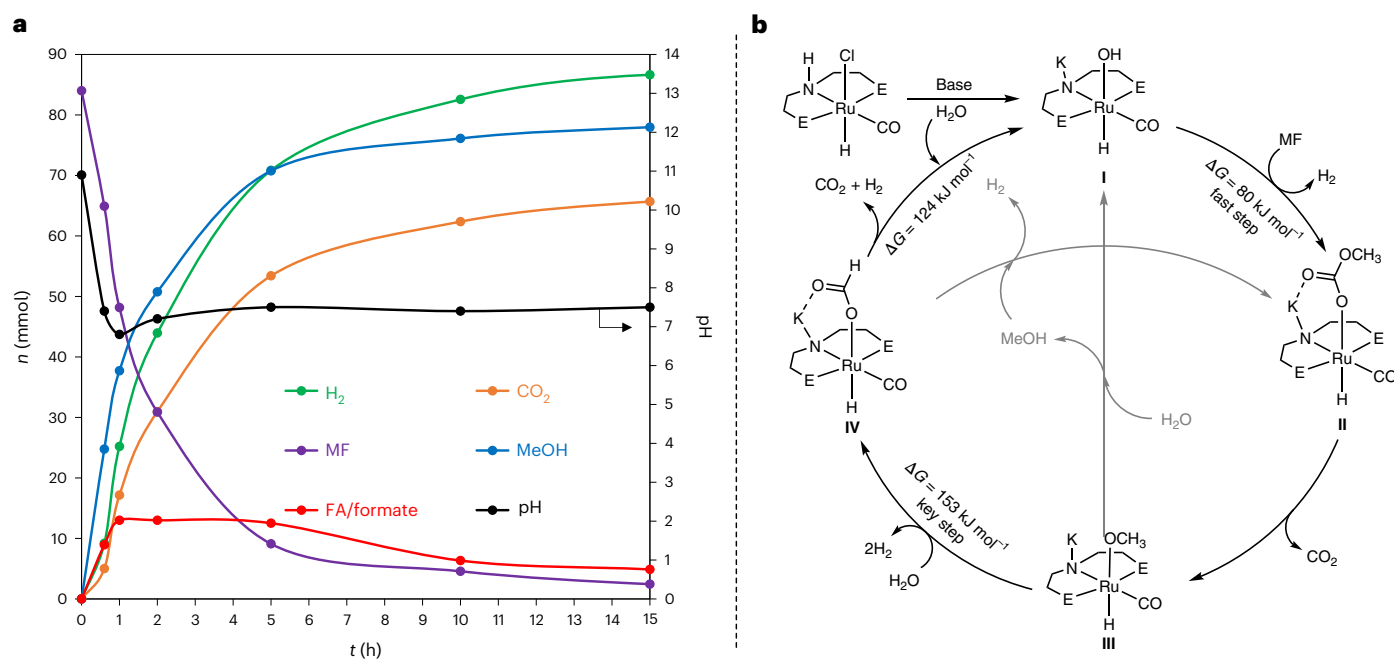


Fig. 4 | Mechanistic investigations of MF dehydrogenation. a, Time course study of compound distribution in MF dehydrogenation. **b**, The proposed catalytic cycle of MF dehydrogenation.

hydrogen, which is of specific interest for combustion or electric engines⁵¹. Using 310 mmol MF in the presence of only 6.5 ppm of catalyst **C5** resulted in a remarkable pressure (70 bar (2 h) and 128 bar (10 h)) (Supplementary Table 21). This corresponds to a catalyst TON(H₂) of >107,000 and TOF(H₂)_{max} of >44,000 h⁻¹. Notably, CO was undetectable in this reaction (Supplementary Fig. 45) and the produced hydrogen could be used directly⁵². Finally, directly using a mixture of the educts MF and H₂O, solvent-free dehydrogenation was performed in a closed autoclave (Supplementary Table 22). Remarkably, a pressure of more than 75 bar was obtained due to gas evolution in the presence of KOH and 25-ppm Ru-catalyst with TON(H₂) > 16,871.

In conclusion, we propose MF as a hydrogen storage material that allows for a carbon-neutral hydrogen energy cycle. Due to its physical and chemical properties, MF complements currently discussed chemical energy carriers. It is available as a multi-million-tonne-scale annual output, has good hydrogen density and is classified as non-toxic, non-irritating and non-corrosive (Fig. 1d). Furthermore, MF can be easily transported, refuelled and handled. In the presence of an appropriate catalyst system, the gas evolution from aqueous MF reforming proceeds five times faster than with FA and 20 times faster than with aqueous MeOH under identical mild conditions. The developed optimal Ru-pincer complex for MF dehydrogenation is highly selective (CO undetectable) and highly active, with TOF(H₂)_{max} > 44,000 h⁻¹ and TON(H₂) > 100,000. Moreover, solvent-free MF dehydrogenation also demonstrates its application potential. Hydrogen generation from MF proceeding by this mechanism is supported by KIE measurements, DFT calculations and X-ray crystal structure and NMR studies.

Methods

Materials and characterization methods

All catalytic experiments were carried out under an Ar or N₂ gas atmosphere with exclusion of air. All liquid reagents were degassed or distilled before use and stored under Ar. All liquid reagents were protected by Ar after distillation or degassed with three freeze–thaw cycles using liquid N₂. Chemicals were purchased from Aldrich, TCI, Alfa, Fisher Chemical, Abcr, Deutero, Eurisotop and Cambridge

Isotope Laboratories. Catalysts **C1–C4**, **C6** and **C7** were purchased from Stem Chemicals. Catalyst **C5** was synthesized according to the procedure reported in ref. 42. Catalyst **C8** was synthesized according to the procedure reported in ref. 53. Air- and moisture-sensitive syntheses were performed under an Ar atmosphere in heating-gun vacuum-dried glassware. The liquid and solid products were characterized by ¹H NMR, ¹³C NMR and ³¹P NMR spectroscopy. The NMR spectra were recorded on Bruker Avance 300 (300 MHz) or 400 (400 MHz) NMR spectrometers. Quantitative ¹³C NMR measurements were performed with a Bruker AV 400-MHz spectrometer, and the analysis time for each sample was no less than 1.5 h. MestReNova (version 14.0.1-23559) was used for interpreting and processing the NMR spectra. Gas chromatography (GC) analysis was performed on an Agilent Technologies 7890A GC system (HP Plot Q/FID, hydrocarbons, Carboxen/TCD, permanent gases; Ar carrier gas), with a CO quantification limit of 78 ppm, and on an Agilent Technologies 7890A GC system (HP Plot Q/FID, hydrocarbons, Carboxen/TCD, permanent gases; He carrier gas), with a CO quantification limit of 10 ppm. pH values were measured on a laboratory digital pH meter (Mettler Toledo AG, SevenEasy pH 8603) at room temperature (24 °C).

Calculation of the hydrogen volume, mole, yield, TON and TOF

The GC was calibrated with certified commercially available gas mixtures. GC samples were taken from the collected gas in the burette after every reaction to obtain the hydrogen percentage (GC_{H₂}) and CO₂ percentage (GC_{CO₂}) in the total gas. The amounts of H₂ and CO₂ (*n*) in mmol were calculated according to

$$n_{\text{H}_2} = \frac{V_{\text{gas}} \times \text{GC}_{\text{H}_2}}{V_{\text{m,H}_2,25^\circ\text{C}}} \quad (1)$$

$$n_{\text{CO}_2} = \frac{V_{\text{gas}} \times \text{GC}_{\text{CO}_2}}{V_{\text{m,CO}_2,25^\circ\text{C}}} \quad (2)$$

The H₂ TON and TOF were calculated by

$$\text{TON}_{\text{H}_2} = \frac{n_{\text{H}_2}}{n_{\text{cat}}} \quad (3)$$

$$\text{TOF}_{\text{H}_2} = \frac{n_{\text{H}_2}}{n_{\text{cat}} \times t} \quad (4)$$

where V_{gas} is the gas volume corrected by the blank volume, and the calculation of standard gas molar volume $V_{\text{m,H}_2,25^\circ\text{C}}$ and $V_{\text{m,CO}_2,25^\circ\text{C}}$ were carried out using

$$V_{\text{m,H}_2,25^\circ\text{C}} = \frac{RT}{p} + b - \frac{a}{RT} = 24.48 \text{ l mol}^{-1} \quad (5)$$

$$V_{\text{m,CO}_2,25^\circ\text{C}} = \frac{RT}{p} + b - \frac{a}{RT} = 24.36 \text{ l mol}^{-1} \quad (6)$$

where $R = 8.3145 \text{ m}^3 \text{ Pa mol}^{-1} \text{ K}^{-1}$, $T = 298.15 \text{ K}$, $p = 101,325 \text{ Pa}$, $a(\text{H}_2) = 24.7 \times 10^{-3} \text{ Pa m}^6 \text{ mol}^{-2}$, $a(\text{CO}_2) = 36.5 \times 10^{-2} \text{ Pa m}^6 \text{ mol}^{-2}$, $b(\text{H}_2) = 26.6 \times 10^{-6} \text{ m}^3 \text{ mol}^{-1}$ and $b(\text{CO}_2) = 42.7 \times 10^{-6} \text{ m}^3 \text{ mol}^{-1}$.

General measurement of MF dehydrogenation

All experiments were performed under an inert atmosphere (N_2 or Ar) with exclusion of air. An amount of one Ru-catalyst with a defined amount of base was added in an autoclave (pressure tube) under an ice bath, followed by certain amount of solvent, MF and H_2O injected by syringe. Next, the autoclave was flushed with N_2 (5 bar) and the pressure was released three times. The reaction was performed at a set temperature for a certain number of hours. The autoclave was then cooled using an ice-bath, and the pressure was carefully released through a room-temperature (25°C) condenser (the water temperature was controlled by a thermostat) to a manual burette to obtain the gas volume. The gas was analysed by GC. Additional CO_2 was collected via burette by adding HCl aqueous solution to the reaction liquid phase.

Data availability

All data generated or analysed during this study are included in this article and the corresponding Supplementary Information data files. Crystallographic data for the structure reported in this article have been deposited at the Cambridge Crystallographic Data Centre, under deposition number CCDC 2162048. Copies of the data can be obtained free of charge via <https://www.ccdc.cam.ac.uk/structures/>. All other data are available from the authors upon reasonable request.

References

- Armaroli, N. & Balzani, V. The future of energy supply: challenges and opportunities. *Angew. Chem. Int. Ed.* **46**, 52–66 (2007).
- Balzani, V. & Armaroli, N. *Energy for a Sustainable World: From the Oil Age to a Sun-Powered Future* (Wiley, 2010).
- Johansson, T. B., Patwardhan, A. P., Nakićenović, N. & Gomez-Echeverri, L. *Global Energy Assessment: Toward a Sustainable Future* (Cambridge Univ. Press, 2012).
- Obama, B. The irreversible momentum of clean energy. *Science* **355**, 126–129 (2017).
- Marks, T. J. et al. Catalysis research of relevance to carbon management: progress, challenges and opportunities. *Chem. Rev.* **101**, 953–996 (2001).
- Roger, I., Shipman, M. A. & Szymes, M. D. Earth-abundant catalysts for electrochemical and photoelectrochemical water splitting. *Nat. Rev. Chem.* **1**, 0003 (2017).
- Schneidewind, J., Cordero, M. A. A., Junge, H., Lochbrunner, S. & Beller, M. Two-photon, visible light water splitting at a molecular ruthenium complex. *Energy Environ. Sci.* **14**, 4427–4436 (2021).
- Hydrogen Economy Outlook* (Bloomberg Finance, 2020).
- A Hydrogen Strategy for a Climate-Neutral Europe*. Report No. 52020DC0301 (European Commission, 2020); <https://eur-lex.europa.eu/legal-content/GA/ALL/?uri=CELEX:52020DC0301>
- Zhou, L. Progress and problems in hydrogen storage methods. *Renew. Sustain. Energy Rev.* **9**, 395–408 (2005).
- Eberle, U., Felderhoff, M. & Schüth, F. Chemical and physical solutions for hydrogen storage. *Angew. Chem. Int. Ed.* **48**, 6608–6630 (2009).
- Niaz, S., Manzoor, T. & Pandith, A. H. Hydrogen storage: materials, methods and perspectives. *Renew. Sustain. Energy Rev.* **50**, 457–469 (2015).
- Kumar, A., Daw, P. & Milstein, D. Homogeneous catalysis for sustainable energy: hydrogen and methanol economies, fuels from biomass, and related topics. *Chem. Rev.* **122**, 385–441 (2022).
- Stavila, V. et al. Nanostructured metal hydrides for hydrogen storage. *Chem. Rev.* **118**, 10775–10839 (2018).
- Hamilton, C. W., Baker, R. T., Staubitz, A. & Manners, I. B–N compounds for chemical hydrogen storage. *Chem. Soc. Rev.* **38**, 279–293 (2009).
- Mellmann, D., Sponholz, P., Junge, H. & Beller, M. Formic acid as a hydrogen storage material—development of homogeneous catalysts for selective hydrogen release. *Chem. Soc. Rev.* **45**, 3954–3988 (2016).
- Sordakis, K. et al. Homogeneous catalysis for sustainable hydrogen storage in formic acid and alcohols. *Chem. Rev.* **118**, 372–433 (2018).
- Bai, S.-T. et al. Homogeneous and heterogeneous catalysts for hydrogenation of CO_2 to methanol under mild conditions. *Chem. Soc. Rev.* **50**, 4259–4298 (2021).
- Onishi, N., Laurenczy, G., Beller, M. & Himeda, Y. Recent progress for reversible homogeneous catalytic hydrogen storage in formic acid and in methanol. *Coord. Chem. Rev.* **373**, 317–332 (2018).
- Wang, W., Wang, S., Ma, X. & Gong, J. Recent advances in catalytic hydrogenation of carbon dioxide. *Chem. Soc. Rev.* **40**, 3703–3727 (2011).
- Boddien, A. et al. Efficient dehydrogenation of formic acid using an iron catalyst. *Science* **333**, 1733–1736 (2011).
- Nielsen, M. et al. Low-temperature aqueous-phase methanol dehydrogenation to hydrogen and carbon dioxide. *Nature* **495**, 85–89 (2013).
- Onishi, N. et al. Development of effective catalysts for hydrogen storage technology using formic acid. *Adv. Energy Mater.* **9**, 1801275 (2019).
- Kar, S., Rauch, M., Leitus, G., Ben-David, Y. & Milstein, D. Highly efficient additive-free dehydrogenation of neat formic acid. *Nat. Catal.* **4**, 193–201 (2021).
- Kothandaraman, J. et al. Efficient reversible hydrogen carrier system based on amine reforming of methanol. *J. Am. Chem. Soc.* **139**, 2549–2552 (2017).
- Kallmeier, F. & Kempe, R. Manganese complexes for (de)-hydrogenation catalysis: a comparison to cobalt and iron catalysts. *Angew. Chem. Int. Ed.* **57**, 46–60 (2018).
- Rossin, A. & Peruzzini, M. Ammonia–borane and amine–borane dehydrogenation mediated by complex metal hydrides. *Chem. Rev.* **116**, 8848–8872 (2016).
- GESTIS Substance Database* (Institut für Arbeitsschutz Deutsche Gesetzliche Unfallversicherung, 2022); <https://gestis-database.dguv.de>
- Zhu, Q.-L. & Xu, Q. Liquid organic and inorganic chemical hydrides for high-capacity hydrogen storage. *Energy Environ. Sci.* **8**, 478–512 (2015).
- Rong, L., Xu, Z., Sun, J. & Guo, G. New methyl formate synthesis method: coal to methyl formate. *J. Energy Chem.* **27**, 238–242 (2018).
- Kaiser, D., Beckmann, L., Walter, J. & Bertau, M. Conversion of green methanol to methyl formate. *Catalysts* **11**, 869 (2021).
- Scott, M. et al. Methylformate from CO_2 : an integrated process combining catalytic hydrogenation and reactive distillation. *Green. Chem.* **21**, 6307–6317 (2019).

33. Federsel, C. et al. A well-defined iron catalyst for the reduction of bicarbonates and carbon dioxide to formates, alkyl formates and formamides. *Angew. Chem. Int. Ed.* **49**, 9777–9780 (2010).
34. Pazicky, M. et al. Preparing methyl formate comprises for example homogeneous-catalyzed reaction of mixture of for example hydrogen, catalyst and tertiary amine compound, phase separation of hydrogenated mixture, and extraction of catalyst residue with the compound. German patent DE102012014159A1 (2013).
35. Schieweck, B. G., Westhues, N. F. & Klankermayer, J. A highly active non-precious transition metal catalyst for the hydrogenation of carbon dioxide to formates. *Chem. Sci.* **10**, 6519–6523 (2019).
36. Corral-Pérez, J. J. et al. Decisive role of perimeter sites in silica-supported Ag nanoparticles in selective hydrogenation of CO₂ to methyl formate in the presence of methanol. *J. Am. Chem. Soc.* **140**, 13884–13891 (2018).
37. Qin, S., Xin, F., Liu, Y., Yin, X. & Ma, W. Photocatalytic reduction of CO₂ in methanol to methyl formate over CuO–TiO₂ composite catalysts. *J. Colloid Interface Sci.* **356**, 257–261 (2011).
38. Chen, J., Xin, F., Qin, S. & Yin, X. Photocatalytically reducing CO₂ to methyl formate in methanol over ZnS and Ni-doped ZnS photocatalysts. *Chem. Eng. J.* **230**, 506–512 (2013).
39. Goepfert, A., Czaun, M., Jones, J.-P., Prakash, G. S. & Olah, G. A. Recycling of carbon dioxide to methanol and derived products—closing the loop. *Chem. Soc. Rev.* **43**, 7995–8048 (2014).
40. Kar, S. et al. Mechanistic insights into ruthenium–pincer-catalyzed amine-assisted homogeneous hydrogenation of CO₂ to methanol. *J. Am. Chem. Soc.* **141**, 3160–3170 (2019).
41. Kar, S., Goepfert, A. S. & Prakash, G. K. S. Integrated CO₂ capture and conversion to formate and methanol: connecting two threads. *Acc. Chem. Res.* **52**, 2892–2903 (2019).
42. Alberico, E. et al. Unravelling the mechanism of basic aqueous methanol dehydrogenation catalyzed by Ru–PNP pincer complexes. *J. Am. Chem. Soc.* **138**, 14890–14904 (2016).
43. Agapova, A., Junge, H. & Beller, M. Developing bicatalytic cascade reactions: ruthenium-catalyzed hydrogen generation from methanol. *Chem. Eur. J.* **25**, 9345–9349 (2019).
44. Gunanathan, C. & Milstein, D. Bond activation and catalysis by ruthenium pincer complexes. *Chem. Rev.* **114**, 12024–12087 (2014).
45. Wei, D., Sang, R., Sponholz, P., Junge, H. & Beller, M. Reversible hydrogenation of carbon dioxide to formic acid using a Mn–pincer complex in the presence of lysine. *Nat. Energy* **7**, 438–447 (2022).
46. Wang, Q. et al. New tricks for an old dog: Grubbs catalysts enable efficient hydrogen production from aqueous-phase methanol reforming. *ACS Catal.* **12**, 2212–2222 (2022).
47. Bielinski, E. A. et al. Base-free methanol dehydrogenation using a pincer-supported iron compound and Lewis acid Co-catalyst. *ACS Catal.* **5**, 2404–2415 (2015).
48. Wang, L. et al. Additive-free ruthenium-catalyzed hydrogen production from aqueous formaldehyde with high efficiency and selectivity. *ACS Catal.* **8**, 8600–8605 (2018).
49. Wu, Y. et al. Nonstoichiometric yttrium hydride—promoted reversible hydrogen storage in a liquid organic hydrogen carrier. *CCS Chem.* **2**, 974–984 (2020).
50. Dubey, A. & Khaskin, E. Catalytic ester metathesis reaction and its application to transfer hydrogenation of esters. *ACS Catal.* **6**, 3998–4002 (2016).
51. Fellay, C., Dyson, P. J. & Laurenczy, G. Viable hydrogen-storage system based on selective formic acid decomposition with a ruthenium catalyst. *Angew. Chem. Int. Ed.* **47**, 3966–3968 (2008).
52. Grasmann, M. & Laurenczy, G. Formic acid as a hydrogen source—recent developments and future trends. *Energy Environ. Sci.* **5**, 8171–8181 (2012).
53. Sung, K. M., Huh, S. & Jun, M. J. Syntheses of ruthenium(II) complexes containing polyphosphine ligands and their applications in the homogeneous hydrogenation. *Polyhedron* **18**, 469–479 (1999).

Acknowledgements

We acknowledge financial support from the European Union, the State of Mecklenburg-Vorpommern. Z.W. acknowledges support from the National Natural Science Foundation of China (22202123). We thank the analytical team of LIKAT (W. Baumann, S. Schareina, S. Buchholz, K. Fiedler, Dipl. Ing. A. Koch and E. F. Krake) for their kind support. We thank the engineers and technicians A. Kammer and A. Hutter for their kind support.

Author contributions

Conceptualization was provided by R.S., P.R., H. Junge and M.B. Catalytic experimental design and results analysis were carried out by R.S., Y.H. and D.W. DFT calculations were performed by Z.W., X.T. and H. Jiao. NMR studies and the SC-XRD experiments were conducted by E.A., R.S., H. Junge and A.S. Equipment assembly was performed by R.S., R.R. and R.J. Funding acquisition was carried out by P.S. and H. Junge. Project administration was performed by P.S., J.M., H. Junge and M.B. Writing (original draft) was carried out by Y.H., R.S., Z.W., E.A. and X.T. Supervision and writing (review and editing) were carried out by M.B., H. Junge, R.S. and H. Jiao. All authors have read and agreed to the published version of this paper.

Funding

Open access funding provided by Leibniz-Institut für Katalyse e.V. (LIKAT Rostock).

Competing interests

The authors declare no competing interests.

Additional information

Supplementary information The online version contains supplementary material available at <https://doi.org/10.1038/s41929-023-00959-8>.

Correspondence and requests for materials should be addressed to Haijun Jiao, Henrik Junge or Matthias Beller.

Peer review information *Nature Catalysis* thanks Ken-ichi Fujita and Yi-An Zhu for their contribution to the peer review of this work.

Reprints and permissions information is available at www.nature.com/reprints.

Publisher's note Springer Nature remains neutral with regard to jurisdictional claims in published maps and institutional affiliations.

Open Access This article is licensed under a Creative Commons Attribution 4.0 International License, which permits use, sharing, adaptation, distribution and reproduction in any medium or format, as long as you give appropriate credit to the original author(s) and the source, provide a link to the Creative Commons license, and indicate if changes were made. The images or other third party material in this article are included in the article's Creative Commons license, unless indicated otherwise in a credit line to the material. If material is not included in the article's Creative Commons license and your intended use is not permitted by statutory regulation or exceeds the permitted use, you will need to obtain permission directly from the copyright holder. To view a copy of this license, visit <http://creativecommons.org/licenses/by/4.0/>.

© The Author(s) 2023